Control of a three-phase four-wire shunt-active power filter based on DC-bus energy regulation

Blaabjerg, Frede; Teodorescu, Remus; Rodriguez, Pedro; Luna, A.; Liserre, Marco

Published in:
11th International Conference on Optimization of Electrical and Electronic Equipment, 2008. OPTIM 2008.

DOI (link to publication from Publisher):
10.1109/OPTIM.2008.4602371

Publication date:
2008

Document Version
Publisher's PDF, also known as Version of record

Control of a Three-phase Four-wire Shunt-Active Power Filter Based on DC-bus Energy Regulation

P. Rodríguez*, A. Luna*, R. Teodorescu**, F. Blaabjerg** and M. Liserre***
* Technical University of Catalonia / Department of Electrical Engineering, Barcelona, Spain
** Aalborg University / Institute of Energy Technology, Aalborg, Denmark
*** Polytechnic of Bari / Electrotechnical and Electronic Eng. Dept., Bari, Italy

***Abstract*— This paper presents a nonconventional three-phase four-wire shunt active power filter (APF) topology controlled by using an energy approach. A general study of power terms involved in the operation of the four-wire APF is conducted in order to evidence the relationship between instantaneous energy stored in the DC bus and active power requirements on the APF. Harmonics and imbalances both on the utility voltage and load current have been considered and the power developed by the active power filter has been evaluated. This study allows designing a controller for the APF based on the regulation of the energy-state of its dc-bus. The method has been experimentally tested on a four leg APF based on a neutral-point-clamped DC bus. Such topology allowed the test of the most general case, including harmonics and imbalance in utility voltage and in load currents.**

I. INTRODUCTION

Two main converter topologies are conventionally employed in three-phase four-wire shunt active power filter (SAPF) applications, namely the four-leg full-bridge (FLFB) topology, and the three-leg neutral-point-clamped (TLNPC) topology. These topologies were presented at the beginning of the 90s [1], and numerous publications on their control have appeared ever since [2]-[4]. The FLFB converter offers high control of its output voltages thanks to its greater number of legs. Nevertheless, interaction between the different legs complicates the modulation process and a non-conventional space-vector modulation technique is necessary in order to achieve suitable reference current tracking [5]. The TLNPC converter, having a smaller number of legs, permits each of the three legs to be controlled independently, making its modulation and current tracking simpler than in the previous topology. However, the dc-bus voltage of the TLNPC converter is not optimally exploited. Moreover, the zero-sequence injected current flows through the dc-bus capacitors. This current gives rise to voltage sharing imbalance in the capacitors, and dc-bus voltage variation, which are undesirable effects in a precise control of the SAPF. Merging FLFB and TLSC topologies as shown in Fig. 1, an alternative four-leg neutral-point-clamped (FLNPC) topology, which solves the cited problems of the previous ones [6]. In this topology, each leg works independently from the other ones, and the current flowing through leg *d* can be regulated in order to achieve no current injected in the dc-bus midpoint; i.e., the dc-bus voltage imbalance can be cancelled.

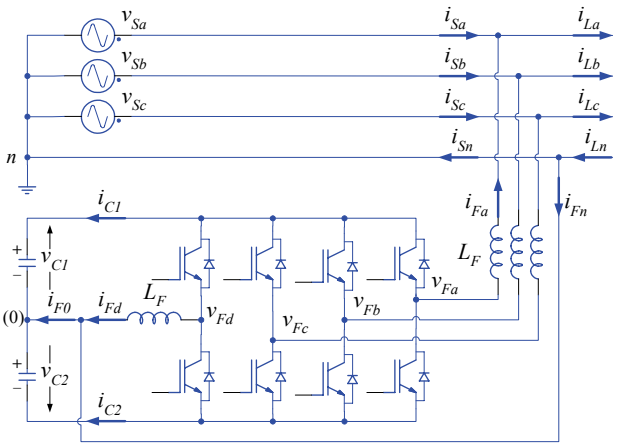

Fig. 1. Four-wire SAPF based on the FLNPC topology

II. AVERAGE MODEL OF THE FLNPC TOPOLOGY

The switching elements in Fig. 1 can be described by a generic switch S shown in Fig. 2, whose control function is exposed in (1).

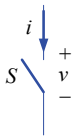

$$s = \begin{cases} 0, i = 0, \text{if } S \text{ is open} \\ 1, v = 0, \text{if } S \text{ is closed} \end{cases} \quad (1)$$

Fig. 2. Generic switch S

Therefore, the logic function describing the behaviour of the two switches of a switching-leg, S_{i1} and S_{i2}, can be written as:

$$s_{i1} + s_{i2} = 1 \;;\; s_{i1} \cdot s_{i2} = 0 \,, \quad (2)$$

and the switching-leg can be represented by a single-pole double-throw switch, as shown in Fig. 3.

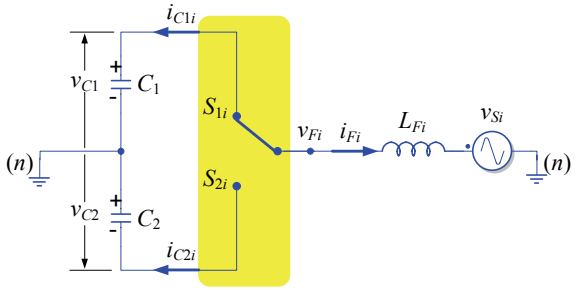

Fig. 3. Switching-led represented as a single-pole, double-throw switch

Supposing C_1=C_2=C, a simple analysis of circuit shown in Fig. 3, allows obtaining state space expressions of (3) for each switching-leg. In these expressions T_{Si} is the switching period, and $d_i \in [0\,,1]$ is the duty cycle of the switching-leg. Therefore, each switching-leg of Fig. 1 can be represented by its state (3a) and output (3b) averaged equations. Variables in (3) represent averaged values, i.e., $i_{Fi} \equiv \bar{i}_{Fi}$, $v_{Si} \equiv \bar{v}_{Si}$, etc.

$$\begin{bmatrix} \dot{i}_{Fi} \\ \dot{v}_{C1} \\ \dot{v}_{C2} \end{bmatrix} = \begin{bmatrix} 0 & \dfrac{d_i}{L_{Fi}} & \dfrac{(1-d_i)}{L_{Fi}} \\ -\dfrac{d_i}{C} & 0 & 0 \\ -\dfrac{(1-d_i)}{C} & 0 & 0 \end{bmatrix} \begin{bmatrix} i_{Fi} \\ v_{C1} \\ v_{C2} \end{bmatrix} + \begin{bmatrix} -\dfrac{1}{L_{Fi}} \\ 0 \\ 0 \end{bmatrix} v_{Si} \quad (3a)$$

$$\begin{bmatrix} v_{Fi} \\ i_{C1} \\ i_{C2} \end{bmatrix} = \begin{bmatrix} 0 & d_i & 1-d_i \\ -d_i & 0 & 0 \\ -(1-d_i) & 0 & 0 \end{bmatrix} \begin{bmatrix} i_{Fi} \\ v_{C1} \\ v_{C2} \end{bmatrix} \quad (3b)$$

From (3b), the duty cycle d_i can be expressed as:

$$d_i = \frac{(v_{Fi} - v_{C2})}{v_{dc}}, \quad (4)$$

where $v_{dc} = v_{C1} - v_{C2}$ is the dc-bus absolute voltage. Substituting (4) in current terms of (3b), and considering the leg output voltage can be written as $v_{Fi} = v_{Si} + L_{Fi}\dot{i}_{Fi}$, then the currents in the capacitors are given by (5).

$$i_{C1} = \frac{1}{v_{dc}}\left(v_{C2} i_{Fi} - v_{Si} i_{Fi} - L_{Fi} i_{Fi} \dot{i}_{Fi}\right) \quad (5a)$$

$$i_{C2} = \frac{1}{v_{dc}}\left(-v_{C1} i_{Fi} + v_{Si} i_{Fi} + L_{Fi} i_{Fi} \dot{i}_{Fi}\right) \quad (5b)$$

From (3), the averaged model of the FLNPC converter can be readily obtained by considering the four averaged switching-legs and the rest of the circuit components. The final state space equations of the FLNPC converter are:

$$\dot{\mathbf{I}}_F = \frac{1}{L_F} \cdot \left(\mathbf{D} \cdot \mathbf{V}_C - \mathbf{V}_S\right) \;\; ; \;\; \dot{\mathbf{V}}_C = -\frac{1}{C} \cdot \mathbf{D}^T \cdot \mathbf{I}_F \;, \quad (6)$$

where $L_{Fi} = L_F \;\forall i\big|_{i=\{a,b,c,d\}}$, C_1=C_2=C, and

$$\mathbf{I}_F = \begin{bmatrix} i_{Fa} & i_{Fb} & i_{Fc} & i_{Fd} \end{bmatrix}^T \;\; ; \;\; \mathbf{V}_C = \begin{bmatrix} v_{C1} & v_{C2} \end{bmatrix}^T \quad (7a)$$

$$\mathbf{V}_S = \begin{bmatrix} v_{Sa} & v_{Sb} & v_{Sc} & 0 \end{bmatrix}^T \;\; ; \;\; \mathbf{D} = \begin{bmatrix} d_a & (1-d_a) \\ d_b & (1-d_b) \\ d_c & (1-d_c) \\ d_d & (1-d_d) \end{bmatrix}. \quad (7b)$$

Expression for current flowing through capacitors in the FLNPC topology is obtained by adding terms as those shown in (5) for each leg and keeping in mind that v_{Sd}=0. Resulting currents are shown in (8), where i_{F0} is the injected current in the dc-bus midpoint, and $p_{F3\phi}$ is the instantaneous active power developed by the converter.

$$i_{C1} = \frac{1}{v_{dc}}\left[v_{C2} i_{F0} - p_{F3\phi} - L_F \sum_{i=a,b,c,d}\left(i_{Fi}\dot{i}_{Fi}\right)\right] \quad (8a)$$

$$i_{C2} = \frac{1}{v_{dc}}\left[-v_{C1} i_{F0} + p_{F3\phi} + L_F \sum_{i=a,b,c,d}\left(i_{Fi}\dot{i}_{Fi}\right)\right] \quad (8b)$$

III. DC-BUS ENERGY VARIATION

From (8), dc-bus energy variation can be expressed as:

$$\begin{aligned} \Delta w_{dc} &= w_{dc} - w_{dc}(0) = \int_0^t \left(v_{C1} i_{C1} + v_{C2} i_{C2}\right) dt \\ &= -\int_0^t \left(p_{F3\phi} + L_F \sum_{i=a,b,c,d} i_{Fi}\dot{i}_{Fi}\right) dt \\ &= -\int_0^t \left(p_{F3\phi} + p_{L_F}\right) dt. \end{aligned} \quad (9)$$

Therefore, energy variation in the dc-bus only depends on the instantaneous active power developed by the filter, $p_{F3\phi}$, and on the instantaneous power associated to the link inductances of the legs, p_{LF}. In a real implementation, there will be additional power consumptions as a consequence of the conduction and switching losses, p_{loss}. Therefore, (9) should be modified in order to obtain:

$$\Delta w_{dc} = -\int_0^t \left(p_{F3\phi} + p_{loss} + p_{L_F}\right) dt \,. \quad (10)$$

Expression (10) evidences the existing linear relationship between energy variation in the dc-bus and power terms affecting to the filter. Therefore, the power supplied by the SAPF of Fig. 1 can be controlled from the estimation of the dc-bus energy variation [7]. This means that, from an energy approach, the SAPF can be represented by means of the block diagram shown in Fig. 4, in which $p_{int} = p_{loss} + p_{LF}$. The controller dedicated to regulate energy variations in the dc-bus, ΔW_{dc}, is studied in §V.

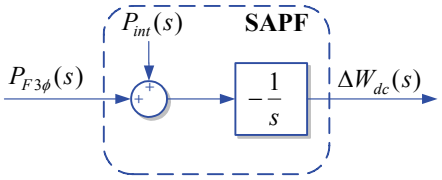

Fig. 4. Energy model of the SAPF

IV. POWER TERMS INVOLVED IN THE SAPF CONTROL

Before designing the controller of the dc-bus energy variation, it is necessary to know the power developed by the SAPF when it is compensating for oscillations in the instantaneous power consumed by a generic load. Under completely general conditions, utility voltage might be unbalanced and distorted; thus, it can be expressed as:

$$\begin{aligned} \begin{bmatrix} v_{L0} \\ v_{L\alpha} \\ v_{L\beta} \end{bmatrix} &= \begin{bmatrix} v_{L0} \\ 0 \\ 0 \end{bmatrix} + \begin{bmatrix} 0 \\ v_{L\alpha}^{+} \\ v_{L\beta}^{+} \end{bmatrix} + \begin{bmatrix} 0 \\ v_{L\alpha}^{-} \\ v_{L\beta}^{-} \end{bmatrix} \\ &= \sum_{n=1}^{\infty} \sqrt{3} \left\{ \sqrt{2} V_{on} \begin{bmatrix} \sin(\omega_n t + \phi_{on}) \\ 0 \\ 0 \end{bmatrix} \right. \end{aligned} \quad (11a)$$

$$+V_{+n}\begin{bmatrix}0\\ \sin(\omega_n t+\phi_{+n})\\ -\cos(\omega_n t+\phi_{+n})\end{bmatrix}+V_{-n}\begin{bmatrix}0\\ \sin(\omega_n t+\phi_{-n})\\ \cos(\omega_n t+\phi_{-n})\end{bmatrix}\Bigg\}, \quad (11b)$$

where V_{+n}, V_{-n} and V_{on} respectively represent the rms values of positive-, negative- and zero-sequence voltage components of the n^{th} harmonic. Likewise, any generic load current might be expressed by means of (12), where I_{+n}, I_{-n} and I_{on} are rms values of each current sequence component.

$$\begin{aligned}\begin{bmatrix}i_{L0}\\ i_{L\alpha}\\ i_{L\beta}\end{bmatrix}&=\begin{bmatrix}i_{L0}\\ 0\\ 0\end{bmatrix}+\begin{bmatrix}0\\ i_{L\alpha}^{+}\\ i_{L\beta}^{+}\end{bmatrix}+\begin{bmatrix}0\\ i_{L\alpha}^{-}\\ i_{L\beta}^{-}\end{bmatrix}\\ &=\sum_{n=1}^{\infty}\sqrt{3}\Bigg\{\sqrt{2}I_{on}\begin{bmatrix}\sin(\omega_n t+\delta_{on})\\ 0\\ 0\end{bmatrix}\\ &+I_{+n}\begin{bmatrix}0\\ \sin(\omega_n t+\delta_{+n})\\ -\cos(\omega_n t+\delta_{+n})\end{bmatrix}+I_{-n}\begin{bmatrix}0\\ \sin(\omega_n t+\delta_{-n})\\ \cos(\omega_n t+\delta_{-n})\end{bmatrix}\Bigg\}\end{aligned} \quad (12)$$

From (11) and (12) the mean value of the instantaneous active power consumed by the load is given by:

$$\begin{aligned}\overline{p}_{L3\phi}=\sum_{n=1}^{\infty}3\Big[&V_{+n}I_{+n}\cos(\phi_{+n}-\delta_{+n})\\ &+V_{-n}I_{-n}\cos(\phi_{-n}-\delta_{-n})+V_{on}I_{on}\cos(\phi_{on}-\delta_{on})\Big]\end{aligned} \quad (13)$$

The mean value of the active power delivered by the source to supply the load and the additional power demanded by the SAPF is given by:

$$\overline{p}_{S3\phi}=\overline{p}_{L3\phi}+\overline{p}_{int}, \quad (14)$$

where the power term corresponding to the internal power demanded by the SAPF, $\overline{p}_{int}$, might represent not only the power losses of the SAPF components, but also any additional load or source connected to the dc-bus, e.g., in the case when the active filtering functionality is implemented in the front-end converter of a three-phase line-interactive PV generation system.

Assuming the line currents drawn from the source as balanced, sinusoidal at fundamental frequency and in phase with the positive sequence voltage of the utility, they could be expressed as:

$$\begin{aligned}\mathbf{I}_S=\begin{bmatrix}i_{S0}\\ i_{S\alpha}\\ i_{S\beta}\end{bmatrix}&=\begin{bmatrix}0\\ i_{S\alpha}^{+1}\\ i_{S\beta}^{+1}\end{bmatrix}=\Big[P\rightarrow I_{\alpha\beta}^{+1}\Big]\begin{bmatrix}0\\ \overline{p}_{S3\phi}\\ 0\end{bmatrix}\\ &=\frac{\overline{p}_{S3\phi}}{\sqrt{3}\,V_{+1}}\begin{bmatrix}0\\ \sin(\omega t+\phi_{+1})\\ -\cos(\omega t+\phi_{+1})\end{bmatrix},\end{aligned} \quad (15)$$

where

$$\Big[P\rightarrow I_{\alpha\beta}^{+1}\Big]=\frac{1}{\left(v_{L\alpha}^{+1}\right)^2+\left(v_{L\beta}^{+1}\right)^2}\begin{bmatrix}0&0&0\\ 0&v_{L\alpha}^{+1}&-v_{L\beta}^{+1}\\ 0&v_{L\beta}^{+1}&v_{L\alpha}^{+1}\end{bmatrix}. \quad (16)$$

In (16), $v_{L\alpha}^{+1}$ and $v_{L\beta}^{+1}$ correspond to the positive sequence utility voltage at fundamental frequency, which could be detected by using an advanced grid synchronization system [8]-[9].

Considering the sinusoidal line currents of (15) under generic voltage conditions, powers supplied by the source side are given by:

$$\begin{aligned}\begin{bmatrix}p_{S0}\\ p_S\\ q_S\end{bmatrix}&=\Big[I_{\alpha\beta0}\rightarrow P\Big]\begin{bmatrix}0\\ i_{S\alpha}^{+1}\\ i_{S\beta}^{+1}\end{bmatrix}=\begin{bmatrix}0\\ \overline{p}_S\\ 0\end{bmatrix}+\begin{bmatrix}0\\ \widetilde{p}_S\\ \widetilde{q}_S\end{bmatrix}=\begin{bmatrix}0\\ \overline{p}_{S3\phi}\\ 0\end{bmatrix}\\ &+\frac{\overline{p}_{S3\phi}}{V_{+1}}\Bigg\{\begin{bmatrix}0\\ \sum_{n=2}^{\infty}V_{+n}\cos\big((n-1)\omega_1 t+\phi_{+n}-\phi_{+1}\big)\\ \sum_{n=2}^{\infty}-V_{+n}\sin\big((n-1)\omega_1 t+\phi_{+n}-\phi_{+1}\big)\end{bmatrix}\\ &-\begin{bmatrix}0\\ \sum_{n=1}^{\infty}V_{-n}\cos\big((n+1)\omega_1 t+\phi_{-n}+\phi_{+1}\big)\\ \sum_{n=1}^{\infty}V_{-n}\sin\big((n+1)\omega_1 t+\phi_{-n}+\phi_{+1}\big)\end{bmatrix}\Bigg\},\end{aligned} \quad (17)$$

where the current-to-power transformation is given by:

$$\Big[I_{\alpha\beta0}\rightarrow P\Big]=\begin{bmatrix}v_{L0}&0&0\\ 0&v_{L\alpha}&v_{L\beta}\\ 0&v_{L\beta}&-v_{L\alpha}\end{bmatrix}. \quad (18)$$

The oscillatory terms in active and reactive powers of (17) are a consequence of the interaction between positive sequence sinusoidal current and all those voltage source components with different frequency and/or sequence. Subtracting instantaneous powers supplied by the source from instantaneous powers consumed by the load, the instantaneous powers developed by the SAPF are:

$$\begin{bmatrix}p_{F0}\\ p_F\\ q_F\end{bmatrix}=\begin{bmatrix}\overline{p}_{F0}\\ \overline{p}_F\\ \overline{q}_F\end{bmatrix}+\begin{bmatrix}\tilde{p}_{F0}\\ \tilde{p}_F\\ \tilde{q}_F\end{bmatrix}=\begin{bmatrix}p_{L0}\\ p_L\\ q_L\end{bmatrix}-\begin{bmatrix}p_{S0}\\ p_S\\ q_S\end{bmatrix} \quad (19a)$$

$$\begin{aligned}\begin{bmatrix}p_{F0}\\ p_F\\ q_F\end{bmatrix}&=\left\{\begin{bmatrix}\overline{p}_{L0}\\ \overline{p}_L\\ \overline{q}_L\end{bmatrix}+\begin{bmatrix}\tilde{p}_{L0}\\ \tilde{p}_L\\ \tilde{q}_L\end{bmatrix}\right\}-\left\{\begin{bmatrix}0\\ \overline{p}_L+\overline{p}_{L0}+\overline{p}_{int}\\ 0\end{bmatrix}+\begin{bmatrix}0\\ \tilde{p}_S\\ \tilde{q}_S\end{bmatrix}\right\}\\ &=\begin{bmatrix}\overline{p}_{L0}\\ -\overline{p}_{L0}-\overline{p}_{int}\\ \overline{q}_L\end{bmatrix}+\begin{bmatrix}\tilde{p}_{L0}\\ \tilde{p}_L-\tilde{p}_S\\ \tilde{q}_L-\tilde{q}_S\end{bmatrix}.\end{aligned} \quad (19b)$$

As a conclusion, the instantaneous active and reactive powers developed by the SAPF are given by:

$$p_{F3\phi}=\widetilde{p}_{L3\phi}-\widetilde{p}_{S3\phi}-\overline{p}_{int}, \quad (20a)$$

$$q_F=\overline{q}_L+\widetilde{q}_L-\widetilde{q}_S. \quad (20b)$$

Therefore, as shown in (20a), the SAPF supplies the load power oscillations, absorbs the source power

oscillations, and consumes the power needed to compensate its internal power consumptions.

From a conventional approach, the SAPF control might be implemented by means of the diagram shown in Fig. 5a. In this figure, the cut-off frequency of the low-pass filter should be selected taking into account that the minimum frequency of oscillations in instantaneous active power consumed by the load can become equal to $2\omega_S$, being ω_S the fundamental utility frequency. Therefore, the transfer function of this low-pass filter is:

$$LPF(s) = \frac{\omega_f^2}{\left(s+\omega_f\right)^2} \quad ; \quad \omega_f = \frac{2\omega_S}{10}. \tag{21}$$

Taking into account that:

$$\begin{aligned} i^*_{Sa,b,c} \cdot v_{La,b,c} &= \overline{p}^*_{S3\phi} + \widetilde{p}^*_{S3\phi} = \overline{p}^*_{L3\phi} + \widetilde{p}^*_{S3\phi}, \\ i_{La,b,c} \cdot v_{La,b,c} &= \overline{p}_{L3\phi} + \widetilde{p}_{L3\phi}, \\ i^*_{Fa,b,c} \cdot v_{La,b,c} &= p^*_{F3\phi}, \end{aligned} \tag{22}$$

the control diagram of Fig. 5a gives rise to the power flow diagram shown in Fig. 5b. In this last diagram, the SAPF energy model has been added in order to describe the energy behavior of the dc-bus. Keeping in mind that $G(s) = -s^{-1}$ and

$$HPF(s) = \left(1 - LPF(s)\right) = \frac{s\left(s+2\omega_f\right)}{\left(s+\omega_f\right)^2}, \tag{23}$$

the analysis of the diagram shown in Fig. 5b conducts to the following expression for the dc-bus energy variation:

$$\Delta W_{dc}(s) = G(s)\left[HPF(s)\cdot P_{L3\phi}(s) + P_{int}(s) - \widetilde{P}^*_{S3\phi}(s)\right]. \tag{24}$$

Transfer function shown in (24) shows as internal power consumptions of the SAPF are not compensated, which is enough reason to justify the necessity of a control loop modification. However, in order to properly establish the control loop modifications, the system will be firstly analyzed considering that $P_{int}(s) - \widetilde{P}^*_{S3\phi}(s) = 0$. Under such operating condition, the transfer function that relates dc-bus energy variation and instantaneous active power of the load is:

$$\frac{\Delta W_{dc}}{P_{L3\phi}}(s) = G(s)HPF(s) = -\frac{s+2\omega_f}{\left(s+\omega_f\right)^2}. \tag{25}$$

In (25), the steady state value of step response is $\Delta w_{dc-ss} = -2/\omega_f$. The need for eliminating this steady state error in the dc-bus energy variation justifies further the need of a suitable energy controller.

V. CONTROLLER OF THE DC-BUS ENERGY VARIATION

The first version of the proposed controller of the dc-bus energy variation is shown in Fig. 6. In this figure, *C(s)* is a proportional controller with a gain equal to *k*, and *H(s)* is constituted by a notch filter in cascade with a low-pass filter tuned at $\omega_h = 2\omega_S$. Its transfer function is:

$$H(s) = \frac{\omega_h^2\left(s^2+\omega_h^2\right)}{\left(s^2+2\xi_h\omega_h s+\omega_h^2\right)^2} \quad ; \quad \omega_h = 2\cdot\omega_S \,,\ \xi_h = 1 \tag{26}$$

Characteristic transfer functions of the proposed controller are shown in (27).

$$\begin{aligned} \frac{P^*_{F3\phi}}{P_{L3\phi}}(s) &= \frac{HPF(s)}{1 - G(s)C(s)H(s)} \\ &= \frac{s^2\left(s+2\omega_f\right)}{\left(1+\dfrac{k\omega_h^2\left(s^2+\omega_h^2\right)}{s\left(s^2+2\xi_h\omega_h s+\omega_h^2\right)^2}\right)\left(s+\omega_f\right)^2} \end{aligned} \tag{27a}$$

$$\frac{\Delta W_{dc}}{P_{L3\phi}}(s) = G(s)\frac{P^*_{F3\phi}}{P_{L3\phi}}(s) \tag{27b}$$

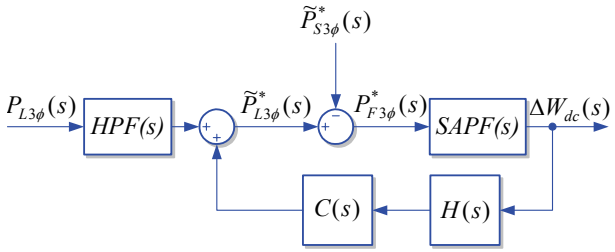

Fig. 6. Initial controller of dc-bus energy variation

Since the whole oscillatory active power of the load at $\omega = 2\omega_S$ should be developed by the SAPF, transfer function shown in (28a) should present unitary gain at this frequency. Thereby, proportional gain is limited to $k = \omega_f$. With this value for *k*, and supposing that *H(s)* block has not been included in the controller, the active power

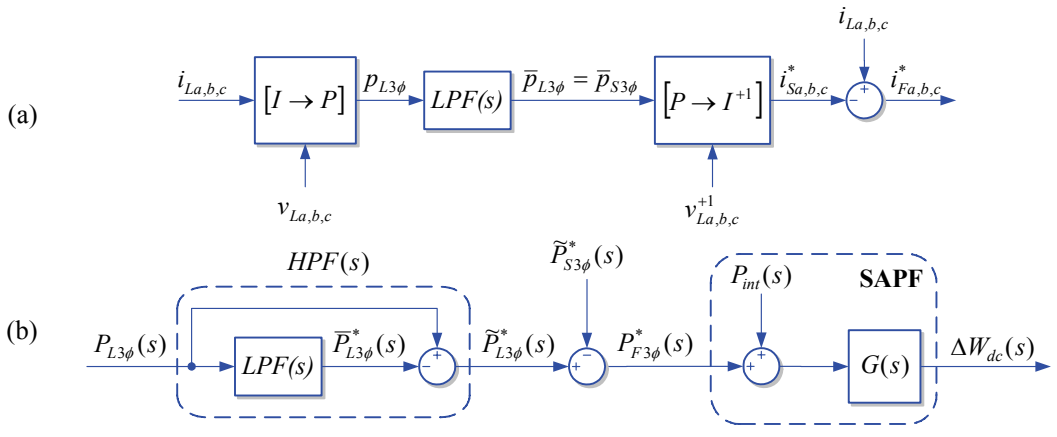

Fig. 5. Conventional SAPF control based on instantaneous active power calculation in the load

consumed by the load at $\omega=2\omega_S$ would be slightly lagged respect to the active power supplied by the SAPF. Hence, an incorrect compensation of this load power component would be performed by the SAPF. To avoid such problem, the *H(s)* block is added to the control loop. Fig. 7 shows temporal evolution of dc-bus energy variation when a unitary step appears in the instantaneous active power consumed by the load. The values set to the control parameters for obtaining this plot were $\omega_S=2\cdot\pi\cdot50$ rad/s, $k=\omega_f=2\cdot\pi\cdot10$ W/J, $\omega_h=2\cdot\pi\cdot100$ rad/s and $\xi_f=\xi_h=1$.

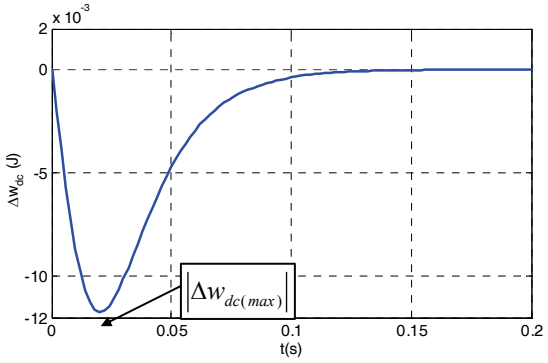

Fig. 7. Step response of the closed-loop system

An analytical study of (27b) permits to obtain a very accurate approximate expression for the maximum absolute value of the waveform plotted in Fig. 7. This expression is shown in (28), where $|\Delta P_L|$ is the absolute value of the load power step.

$$\left|\Delta w_{dc(max)}\right| = \frac{\left|\Delta P_L\right|}{k\left(1-2\xi_h\dfrac{\omega_f}{\omega_h}\right)}\left(1+\sqrt{2}\right)e^{-\sqrt{2}} \tag{28}$$

If it is supposed that current injected by the converter leg *d* is properly controlled in order to achieve balance in the dc-bus voltage sharing [10]-[11], then energy stored in the dc-bus can be calculated by:

$$w_{dc} = \frac{1}{4}C\left(v_{C1}-v_{C2}\right)^2 = \frac{1}{4}Cv_{dc}^2\,, \tag{29}$$

where v_{dc} is the dc-bus absolute voltage and $C_1=C_2=C$. Therefore, dc-bus energy variation regarding an initial value adopted as a reference would be:

$$\Delta w_{dc} = \frac{1}{4}C\left(v_{dc}^2 - v_{dc(ref)}^2\right), \tag{30}$$

where $v_{dc(ref)}$ is the dc-bus voltage adopted as a reference. From (28) and (30), it is possible to determinate the proper value for the dc-bus capacitors in order to ensure that dc-bus absolute voltage does not overpass a limit value, $v_{dc(lim)}$, when a certain load power step appears.

$$C \geq \frac{4\cdot\left|\Delta w_{dc(max)}\right|}{\left|v_{dc(ref)}^2 - v_{dc(lim)}^2\right|} \tag{31}$$

So far, it has been considered that $P_{int}(s)-\widetilde{P}^*_{S3\phi}(s)=0$. If now these power terms are kept in mind, an analysis of the diagram shown in Fig. 6 allows obtaining the expression of (32) for dc-bus energy variation.

$$\Delta W_{dc}(s) = \frac{G(s)}{1-G(s)C(s)H(s)}\Big[HPF(s)P_{L3\phi}(s) + \left(P_{\text{int}}(s)-\widetilde{P}^*_{S3\phi}(s)\right)\Big] \tag{32}$$

In (32), no all of the power terms affect in the same way over the dc-bus energy variation. Taking into account that internal power consumptions can become important when additional loads/sources are connected to the dc-bus, it should be interesting to have a unique transfer function which univocally relates all of the power terms with the dc-bus energy variation. To achieve this goal, a second control loop is added to the initial controller. Fig. 8 shows the new structure of the dc-bus energy variation controller. In this diagram, real structure of the high-pass filter has been considered, *D(s)=s* is a derivative block, and *LPF(s)* is the low-pass filter shown in (21). Besides, a new power magnitude has been defined, $P_{F(eff)}(s)$, which corresponds to the effective power which effectively modifies the energy stored in the dc-bus. Analyzing the diagram shown in Fig. 8, the following transfer function is obtained:

$$\frac{\Delta W_{dc}}{P_{L3\phi}+P_{\text{int}}-\widetilde{P}^*_{S3\phi}}(s) = HPF(s)\frac{G(s)}{1-G(s)C(s)H(s)}\,. \tag{33}$$

Expression of (33) denotes that dc-bus energy variation is completely controlled, following an identical evolution versus variations in any of the powers that affect to the energy state of the dc-bus. Analyzing control diagram shown in Fig. 8 is obtained that:

$$\frac{\overline{P}^*_{L3\phi}(s)}{\Delta W_{dc}(s)} = -\frac{H(s)C(s)+D(s)LPF(s)}{1-LPF(s)} = -\left[H(s)C(s)F_1(s)+F_2(s)\right], \tag{34}$$

where $F_1(s)$ and $F_2(s)$ are defined by:

$$F_1(s) = \frac{1}{1-LPF(s)} = 1+\frac{\omega_f^2}{s\left(s+2\omega_f\right)} \tag{35a}$$

$$F_2(s) = D(s)\frac{LPF(s)}{1-LPF(s)} = \frac{\omega_f^2}{s+2\omega_f} \tag{35b}$$

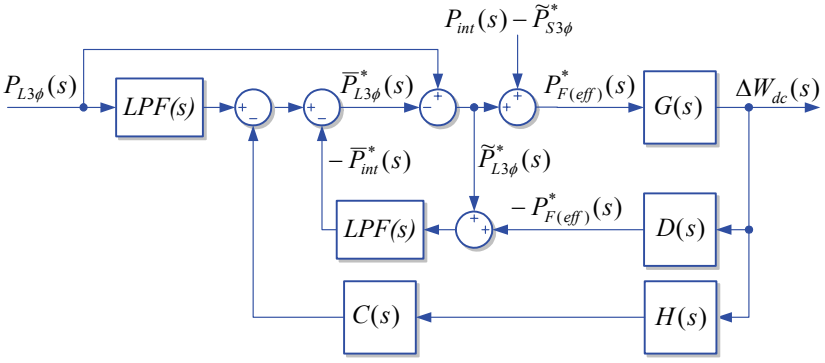

Fig. 8. Control diagram of the dc-bus energy variation controller using a double feedback loop

Expression (34) leads to the definitive diagram, shown in Fig. 9, for the SAPF controller based on the dc-bus energy regulation.

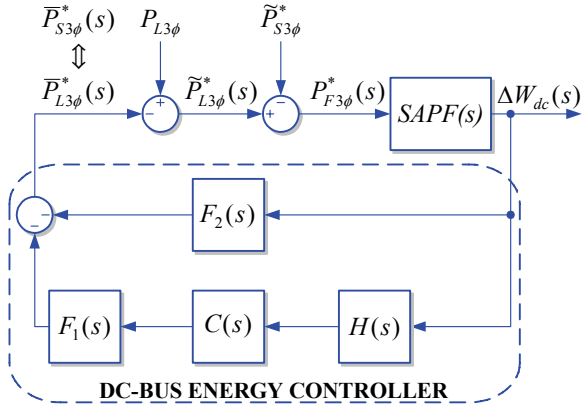

Fig. 9. Definitive SAPF controller diagram

Implementation of this definitive SAPF control diagram is shown in Fig. 10, where the reference current for leg *d* is obtained by means of $i^*_{Fd} = -\left(i^*_{Fa} + i^*_{Fb} + i^*_{Fc}\right)$, and power to current transformation is given by:

$$i^*_{Si} = \left[P \rightarrow I^{+1}\right] \cdot v^{+1}_{Si}\Big|_{i=a,b,c} \quad ; \quad \left[P \rightarrow I^{+1}\right] = \frac{\overline{p}^*_{L3\phi}}{\sum_{j=a,b,c}\left(v^{+1}_{Sj}\right)^2} \cdot \quad (36)$$

In Fig. 10, the dc-bus energy variation is calculated by means of (30) from the dc-bus absolute voltage sensing. This is the input variable of the dc-bus energy controller, and its output variable is the mean value of the instantaneous active power that should be supplied by the source. This value of power acts as an input for the power to current transformation. The other input of this transformation is the positive sequence utility voltage at fundamental frequency, which is obtained from an advanced PLL/FLL [8][9]. The output of this transformation is the set of purely active sinusoidal currents that should flow from the source side. Subtracting this source reference current from the instantaneous load current, the reference current for the SAPF is obtained.

VI. Experimental Results

An APF prototype based on FLNPC topology was been implemented for experimental validation purposes. This APF should compensate current harmonics in a weak network (with high impedance on the source side). A single-phase full-bridge uncontrolled rectifier connected between a phase and neutral conductors has been considered as a load. Figure 11 shows source currents and voltages at the point of common coupling (PCC) between the load and the utility when APF is unconnected. In this figure, it can be appreciated as voltages at the PCC, besides distorted, are unbalanced as a consequence of the unbalanced currents consumed by the three phases of the load. These unbalanced voltages would negatively affect on any third load connected at the PCC, e.g. on a three-phase induction motor. This unbalanced voltage consists of positive and negative-sequence components, which would give rise to power and torque oscillations in the motor.

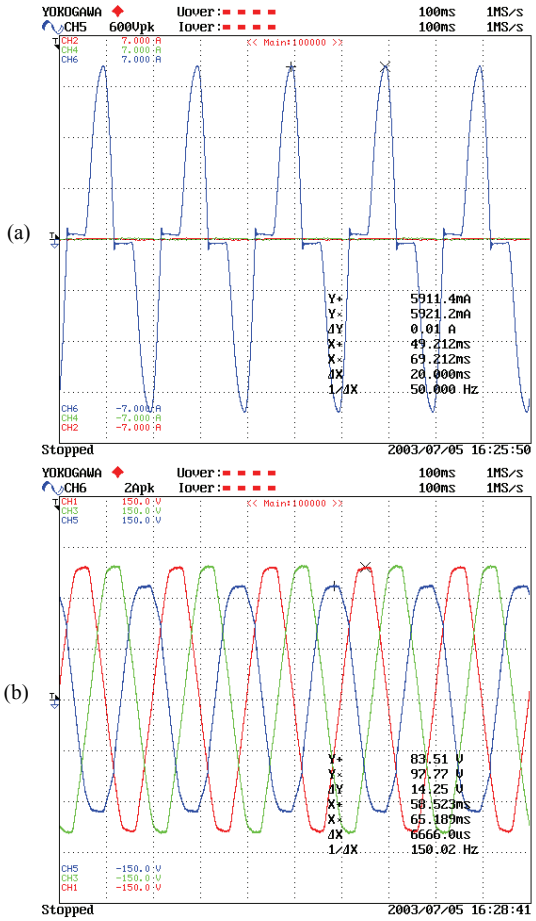

Fig. 11. (a) Load currents. (b) Voltages at the PCC.

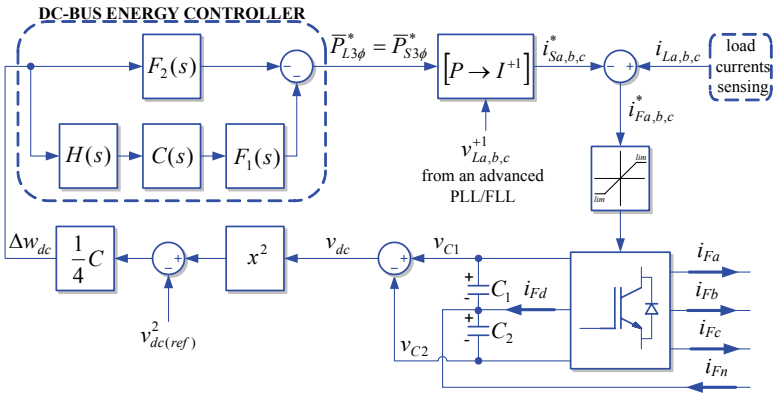

Fig. 10. Implementation of the SAPF controller by means of dc-bus energy regulation

In a first experiment, the load currents sensing block of Fig. 10, which provided $i_{La,b,c}$, was been intentionally disabled on the connection of the APF to the utility. Consequently, the APF will only request those necessary currents to compensate its internal power losses. Figure 12(a) shows the source current under such operating conditions. In this case, the source current was composed by the original load current, plus a set of balanced sinusoidal currents destined to compensate the internal losses of the APF.

When load current sensing block was enabled in Fig. 10, the APF injects the proper currents in the utility to conditioning the currents consumed by the load.

Figure 12(b) shows the conditioned source currents. Obviously, the mean value of instantaneous active supplied by the source by means these currents coincides with the mean value of instantaneous active power consumed by the load and by the APF.

Figure 12(c) shows as, once load currents have been conditioned, voltages at the PCC are balanced. In this case, as the source side impedance is high, a high frequency component appears superposed on the grid voltages waveforms. This high frequency component is due to the portion of the high frequency current ripple injected into the grid, which can not attenuated by the passive filter connected on the output of the APF in this experiment.

VII. Conclusion

From the study presented in this paper, it can be concluded that the proposed controller provides an effective method for reference currents calculation, based on energy state of the SAPF. Analyzing the SAPF from an energy approach, conventional capabilities can be extended, and it is possible to add the active filtering function to the conventional three-phase PWM boost rectifiers. With this approach, dc-bus capacitors are rated according to dynamic response of the system; therefore, operation conditions of the SAPF can be assured versus sudden variations in load power.

References

[1] *C.A. Quinn and N. Mohan, "Active Filtering Currents in Three-Phase, Four-Wire Systems with Three-Phase and Single-Phase Non-Linear Loads," in Proc. IEEE- APEC, pp. 829-836, Feb. 1992.*

[2] *S. Buso, L. Malesani, and P. Mattavelli, "Comparison of Current Control Techniques for Active filter Applications," IEEE Trans. Industrial Electronics, Vol. 45, No. 5, pp. 722-729, Oct. 1998.*

[3] *P. Verdelho and G.D. Marques, "Four-Wire Current-Regulated PWM Voltage Converter," IEEE Trans. Industrial Electronics, Vol. 45, No. 5, pp. 761-770, Oct. 1998.*

[4] *R. Zhang, V.H. Prasad, D. Boroyevich and F.C. Lee, "Three-Dimensional Space Vector Modulation for Four-Leg Voltage-Source Converters," IEEE Trans. Power Electronics, Vol. 17, No. 3, pp. 314-326, May 2002.*

[5] *A. Quinn and N. Mohan, "Active Filtering Currents in Three-Phase, Four-Wire Systems with Three-Phase and Single-Phase Non-Linear Loads," in Proc. IEEE- APEC, pp. 829-836, Feb. 1992.*

[6] *S. Buso, L. Malesani, and P. Mattavelli, "Comparison of Current Control Techniques for Active filter Applications," IEEE Trans. Industrial Electronics, Vol. 45, No. 5, pp. 722-729, Oct. 1998.*

[7] *P. Verdelho and G.D. Marques, "Four-Wire Current-Regulated PWM Voltage Converter," IEEE Trans. Industrial Electronics, Vol. 45, No. 5, pp. 761-770, Oct. 1998.*

[8] *R. Zhang, V.H. Prasad, D. Boroyevich and F.C. Lee, "Three-Dimensional Space Vector Modulation for Four-Leg Voltage-Source Converters," IEEE Trans. Power Electronics, Vol. 17, No. 3, pp. 314-326, May 2002.*

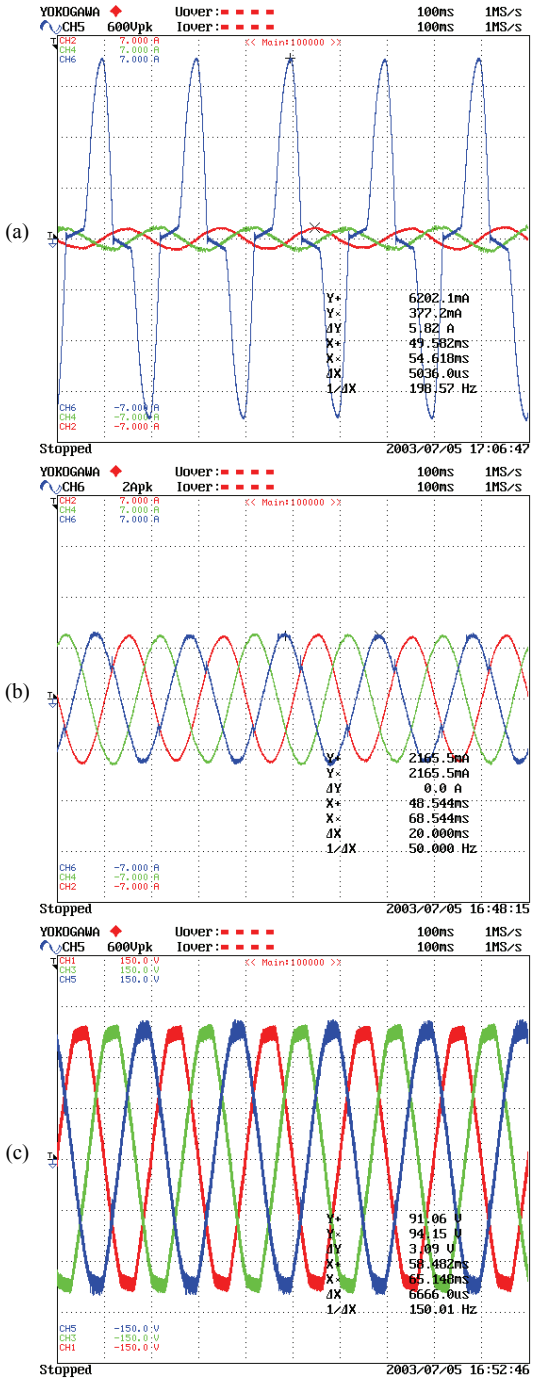

Fig. 12. (a) Source current supplying the load and the APF power losses. (b) Conditioned source currents. (c) Balanced voltages at the PCC.

[9] *M. A. Perales, M. M. Prats, R. Portillo, José L. Mora, J. I. León, and L. G. Franquelo, "Threedimensional space vector modulation in abc coordinates for four-leg voltage source converters," IEEE Power Electron. Letters, vol. 45, pp. 104-109, Dec. 2003.*

[10] *P. Rodríguez, R. Pindado and J. Bergas, "Alternative Topology for Three-Phase Four-Wire PWM Converters Applied to a Shunt Active Power Filter," in Proc. IEEE-IECON, Vol. 4, pp. 2939-2944, Nov. 2002.*

[11] *P. Rodríguez, R. Pindado and J. Pou, "Energy Control of Three-phase Four-wire Shunt Active Power Filter," in Proc. IEEE-IECON, pp. 1061-1066, Nov. 2003.*

[12] *P. Rodriguez, , J. Pou, J. Bergas, J.I. Candela, R.P. Burgos, D. Boroyevich, "Decoupled Double Synchronous Reference Frame PLL for Power Converters Control," IEEE Trans. on Power Electron., vol.22, no.2, pp.584-592, March 2007.*

[13] *P. Rodriguez, A. Luna, M. Ciobotaru, R. Teodorescu, F. Blaabjerg, "Advanced Grid Synchronization System for Power Converters under Unbalanced and Distorted Operating Conditions," in Proc. IEEE-IECON, pp.5173-5178, Nov. 2006.*

[14] *Q.-C. Zhong, T.C. Green, J. Liang and G. Weiss, "H∞ Control of the Neutral Point in 3-phase 4-wire DC-AC Converters," in Proc. IEEE-IECON, Vol. 1, pp. 520-525, Nov. 2002.*

[15] *M.K. Mishra, A. Joshi and A. Ghosh, "Control Schemes for Equalization of Capacitor Voltages in Neutral Clamped Shunt Compensator," IEEE Trans. Power Delivery, Vol. 18, No. 2, pp. 538-544, April 2003.*

[16] *M. Liserre, F. Blaabjerg, S. Hansen, "Design and control of an LCL-filter-based three-phase active rectifier," IEEE Trans. Industry Applicat. , vol.41, no.5, pp. 1281-1291, Sept.-Oct. 2005*